Electronic Supplementary Information

Integration of a Bulky Adamantane Unit with 9-Phenyl-9H-3,9'-Bicarbazole: A Novel Host Design for Solution-Processed Narrowband TADF-OLEDs

Haeun Kwak, Nagaraju Peethani , Su Hong Park, Na Yeon Kwon, Jin Young Park, Min Ji Kang, Chae Yeong Park, Ha Yeon Kim, Chang Seop Hong, Sungnam Park, Min Ju Cho*, and Dong Hoon Choi*

[a] Department of Chemistry, Research Institute for Natural Sciences, Korea University, 145 Anam-ro, Seongbuk-gu, Seoul, 02841, Republic of Korea.

General techniques and materials

Characterization and measurements

The UV-visible absorption spectra of the molecules dissolved in toluene and cast into thin films were analyzed using an Agilent 8453 UV-visible absorption spectrometer equipped with a photodiode array covering the wavelength range of 190–1100 nm. Fluorescence spectra at 77 K and 298 K and phosphorescence spectra at 77 K with a delay time of 1.0 ms were obtained using an F-7100 fluorescence spectrophotometer (HITACHI). Proton nuclear magnetic resonance (^{1}H NMR) spectra at 500 MHz and carbon nuclear magnetic resonance (^{13}C NMR) at 125 MHz were acquired in $CDCl_3$ using a Varian Mercury spectrometer from Cambridge Isotope Laboratories, Inc. The masses of the synthesized compounds were determined utilizing matrix-assisted laser desorption ionization time-of-flight (MALDI-TOF) mass spectrometry, specifically the MALDI-TOF/TOF™ 5800 system by AB SCIEX, at the Korea Basic Science Institute (Seoul). Elemental analysis was conducted using a FlashSmartTM elemental analyzer (Thermo Fisher Scientific). The thermal properties, including the glass transition temperature (T_g) and melting temperature (T_m) of the emitters, were determined in an N_2 atmosphere using differential scanning calorimetry (DSC, Mettler STARe). The materials' thermal decomposition temperature (T_d) was confirmed via

thermogravimetric analysis (TGA, Mettler STARe, heating rate of 10 °C min^{-1}, N_2 conditions). The electrochemical properties of the hosts in the films were measured using cyclic voltammetry with a potentiostat (EA161, eDAQ) at a scan rate of 50mV s^{-1} to determine the oxidation potentials. The absolute photoluminescence quantum yields (PLQYs) of the films were determined using an integrating sphere (ILF-835) equipped with an FP-8500 spectrofluorometer (JASCO). The film roughness was measured by AFM (Park Systems, XE-100) in non-contact mode.

Theoretical calculations

Density functional theory (DFT) and time-dependent density functional theory (TD-DFT) calculations were performed using the Gaussian 16 software package with the B3LYP functional and 6-31G(d) basis set. The polarizable continuum model with integral equation formalism (IEFPCM) was used for solvation (toluene). The HOMO and LUMO were obtained from the optimized structures of the molecules in the ground state. The vertical electronic excitation energies (S_1 and T_n states) were obtained by calculating the Franck-Condon transition from the ground state to the corresponding electronic excited states using TD-DFT calculations. Additionally, the natural transition orbitals (NTOs) for the electronic transitions were calculated to examine the electron and hole wave functions and characterize the electronic absorption properties.

Time-resolved electroluminescence (TREL)

Time-resolved electroluminescence (TREL) signals were obtained by applying voltage pulses (100 Hz and 1 ms pulse width) to the OLED devices built into a jig (McScience) using an arbitrary

function generator (AFG31021, Tektronix). The TREL signals were collected using a photomultiplier tube (PMT). The rising and falling times of the voltage pulses were both 4 ns, which is sufficiently short to investigate the exciton and polaron dynamics. The voltage drop across a shunt resistor of 50 Ω, connected in series with the devices, was measured using an oscilloscope at high impedance to measure the current through the devices. For the TREL measurements, the voltage pulse of 4.5 V was used. [S1, S2]

Single carrier devices

To compare their charge carrier transport abilities, host-containing HODs were fabricated on patterned ITO-coated glass (serving as the anode) with a sheet resistance of Ω cm^{-2} (AMG Corp.). The HOD configurations were as follows: ITO (150 nm)/ PEDOT: PSS (30 nm)/ PX2Cz (20 nm)/ EML (20 nm)/ Al (100 nm). PEDOT: PSS was deposited as received and annealed at 155 °C for 15 min, whereas crosslinked PX2Cz was annealed at 130 °C for 20 min. The blended solution of the host and 4FlCzBN was spin-coated as required. Al were then deposited using a thermal evaporator.

OLED device fabrication

OLED devices were fabricated on glass substrates coated with a transparent ITO layer (150 nm) as the anode, with a sheet resistance of 15 Ω cm^{-2} and an active pattern size of 2 × 2 mm^2. The substrates were cleaned in distilled water for 10 min, isopropanol for 20 min, and isopropanol (HPLC) for 20 min using an ultrasonic bath and dried using hot air. PEDOT: PSS was directly

spin-coated onto an ITO plate to form a hole injection layer (30 nm) and heated at 155 °C for 15 min on a hot plate. PX2Cz was dissolved in chlorobenzene using a photoacid generator and spin-coated to form a hole-transporting layer (20 nm). Subsequently, PX2Cz was photocrosslinked with 254nm light heated at 130 °C for 20 min on a hot plate. A mixture of the host and 4FlCzBN (4 wt% ratio, 1 wt% in toluene) was spin-coated to form an emitting layer. BmPyPB (50 nm) was used as the electron-transporting layer, and LiF (1 nm) and Al (100 nm) were vacuum-deposited in an inert chamber under a pressure of 5×10^{-6} Torr. The fabricated device structure consisted of ITO (150 nm), PEDOT: PSS (30 nm), PX2Cz (20 nm), host 4FlCzBN (20 nm), BmPyPB (50 nm), LiF (1 nm), and Al (100 nm). The fabrication was performed under ambient conditions before the substrates were placed in a thermal vacuum evaporator to evaporate the BmPyPB, LiF, and Al.[S3, S4]

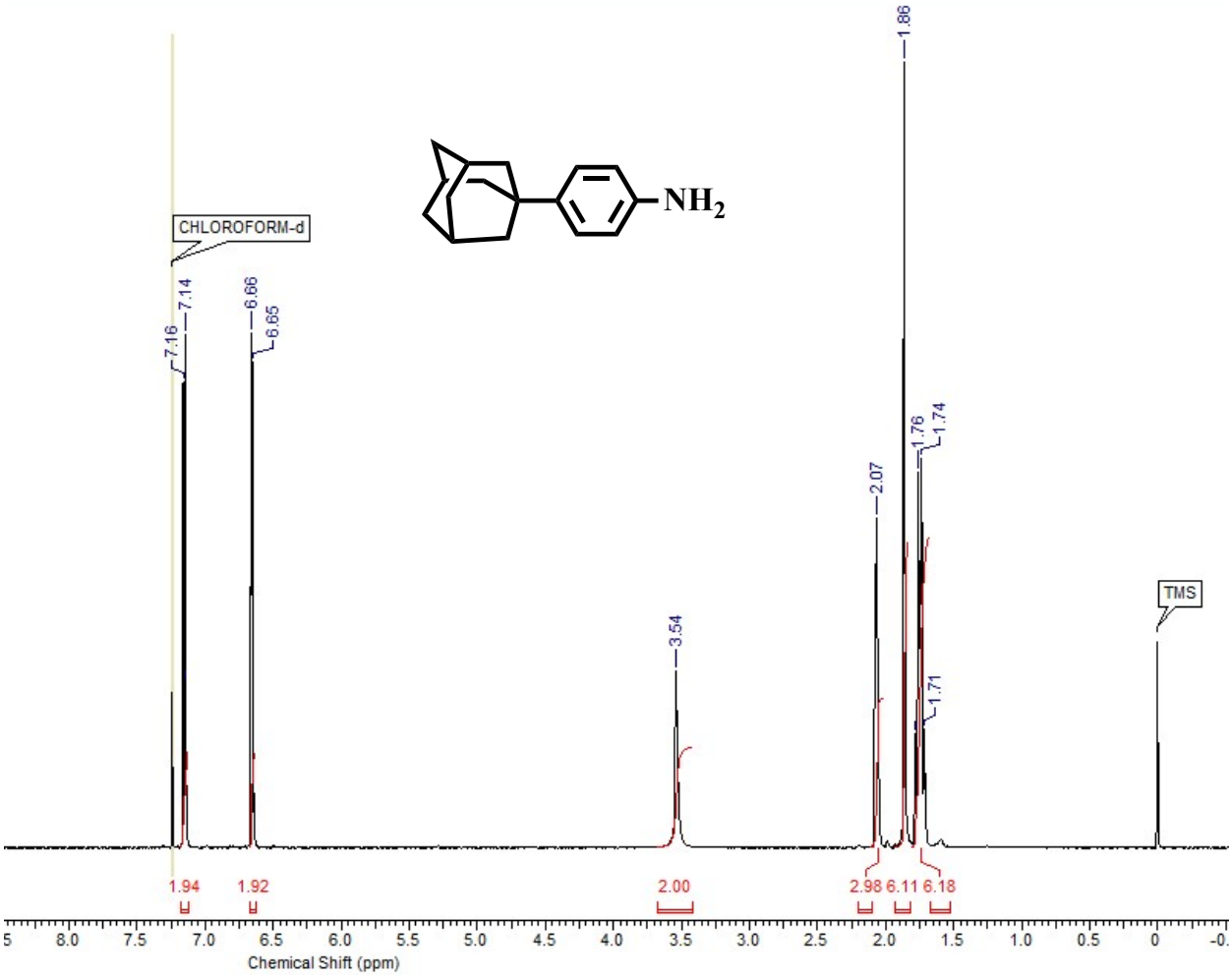

Fig. S1 ^{1}H NMR spectrum of **4-((1s,3s)-adamantan-1-yl)aniline**.

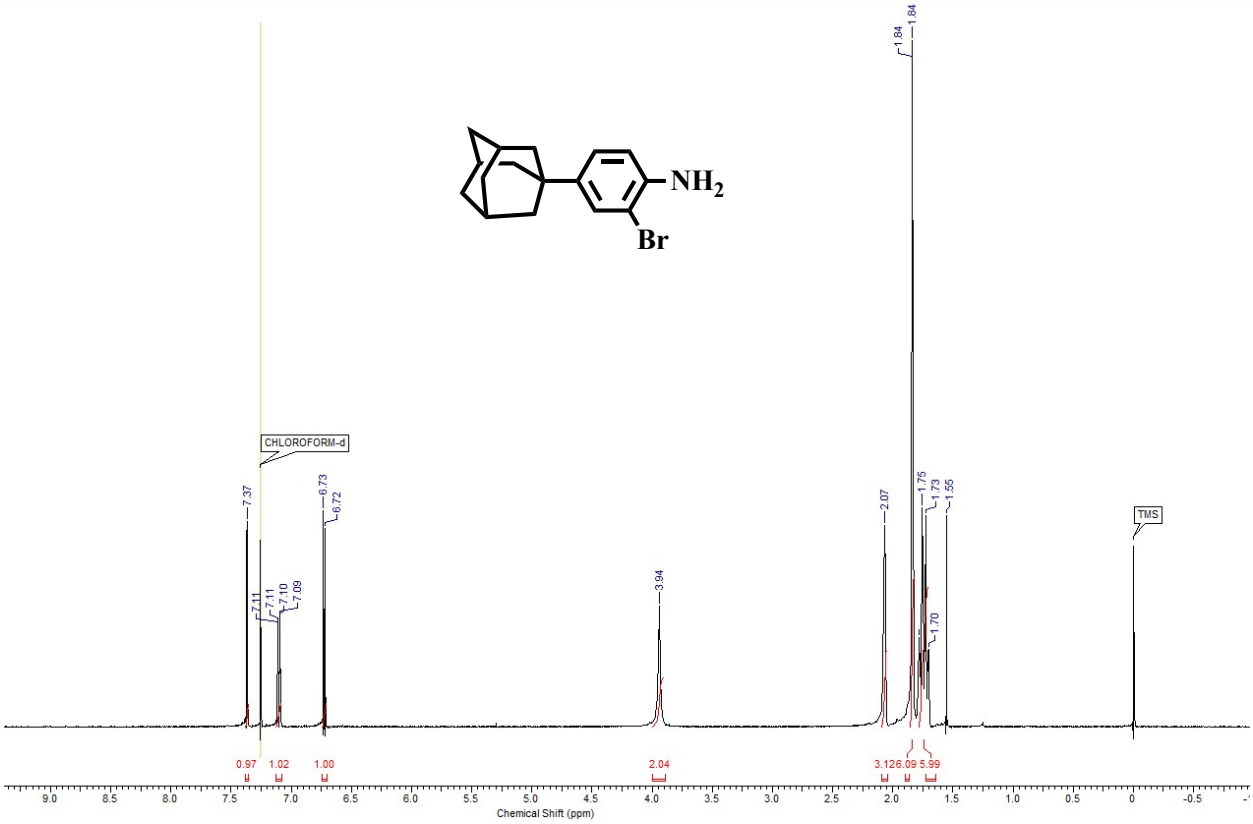

Fig. S2 ^{1}H NMR spectrum of **4-((1s,3s)-adamantan-1-yl)-2-bromoaniline**.

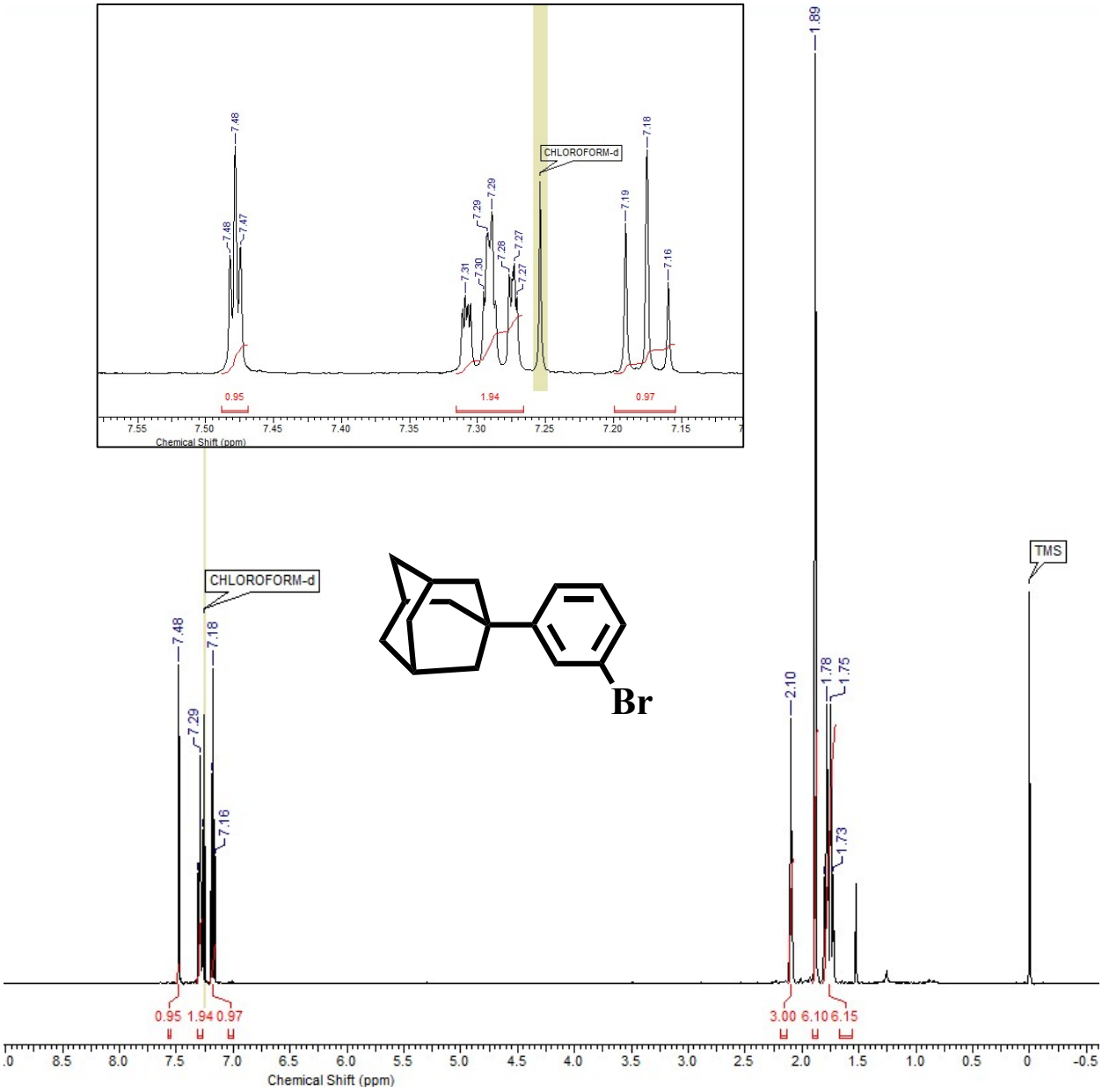

Fig. S3 ^{1}H NMR spectrum of **(1s,3s)-1-(3-bromophenyl)adamantane** .

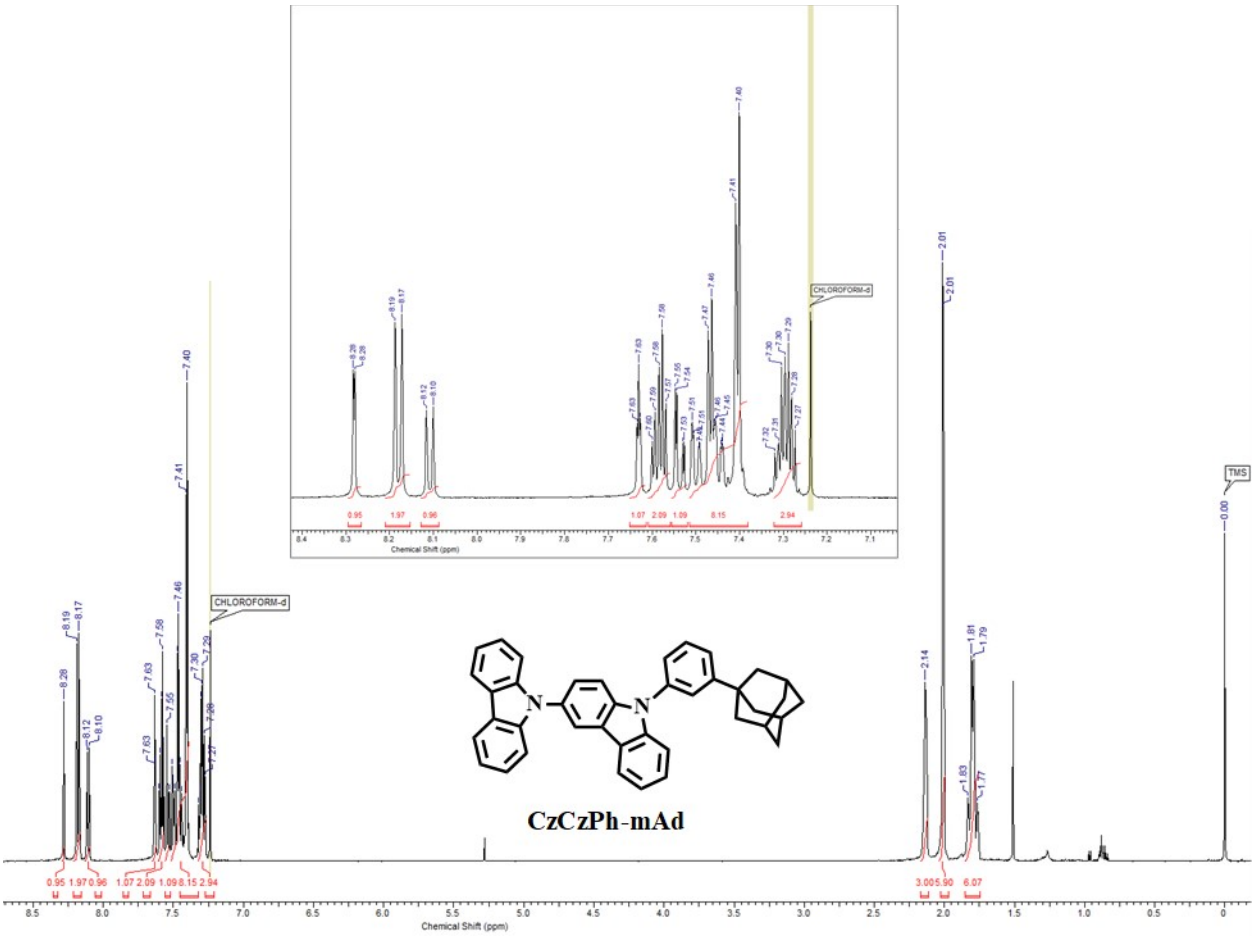

Fig. S4 ^{1}H NMR spectrum of **CzCzPh-mAd**.

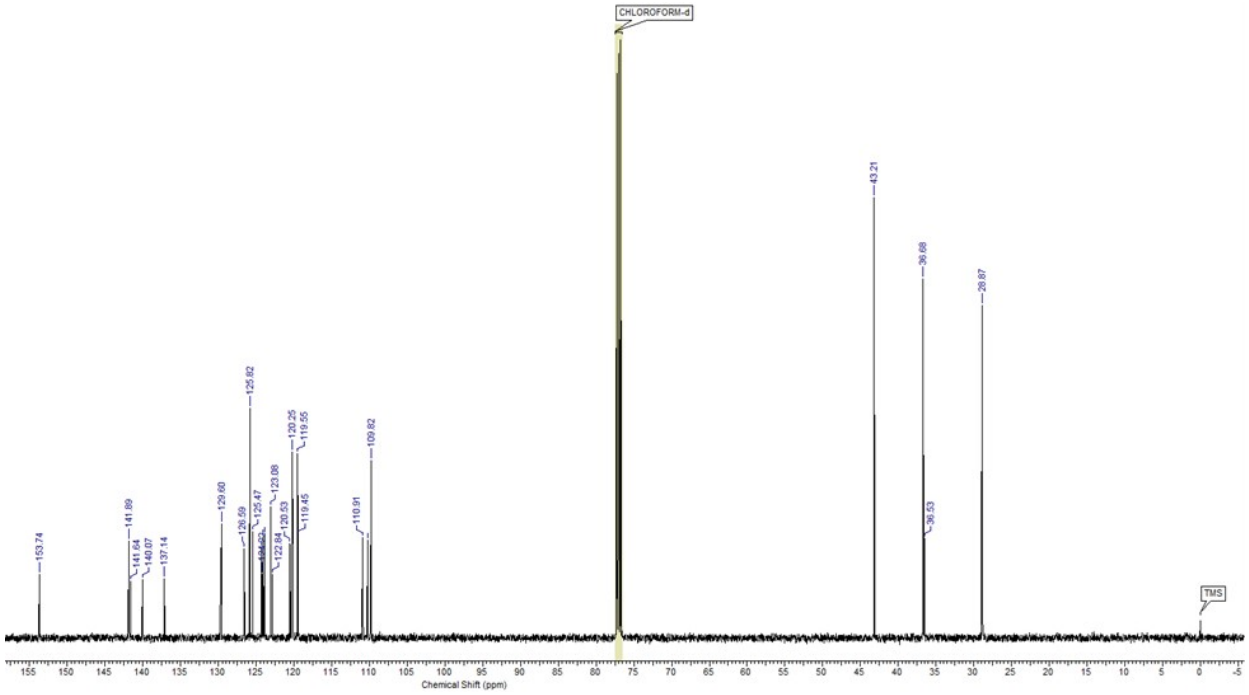

Fig. S5 ^{13}C NMR spectrum of **CzCzPh-mAd**.

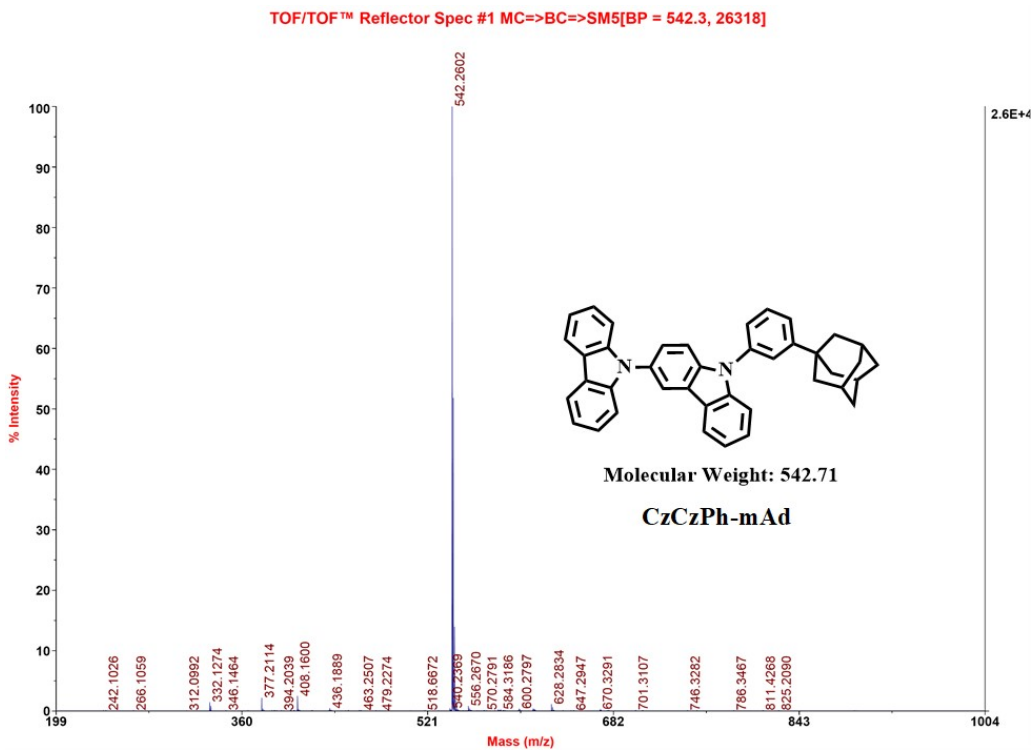

Fig. S6 MALDI-TOF spectrum of **CzCzPh-mAd**.

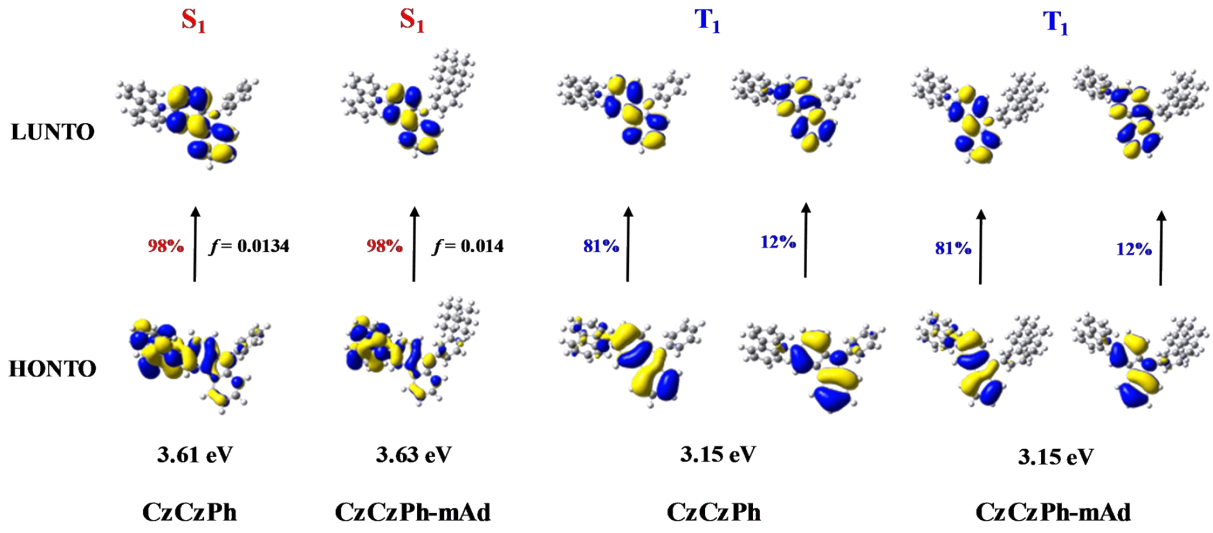

Fig. S7 Calculated HONTO and LUNTO for $S_0 \rightarrow S_1$ and $S_0 \rightarrow T_1$ transitions of CzCzPh and **CzCzPh–mAd** were obtained by DFT calculations (B3LYP/6-31G(d)). NTOs of CzCzPh and

CzCzPh–mAd are almost identical, indicating that the adamantane unit makes no significant changes to the electronic and optical properties of CzCzPh.

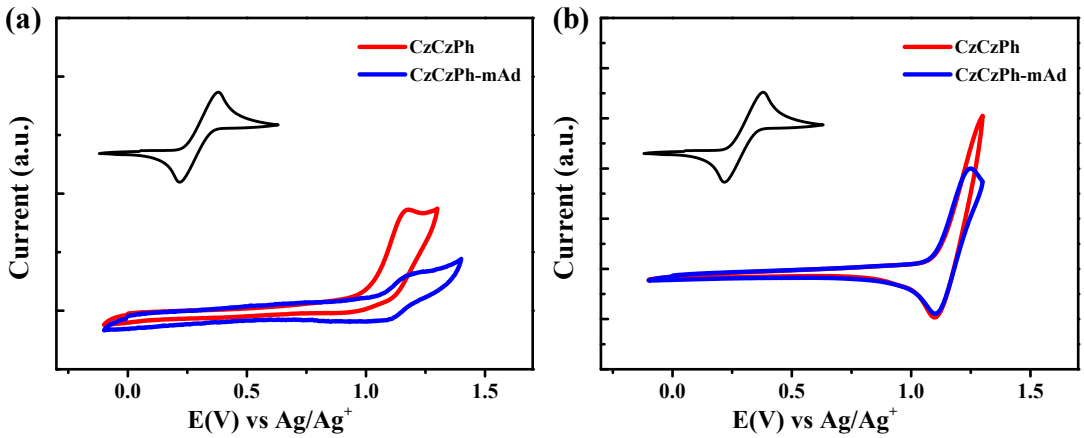

Fig. S8 Cyclic voltammograms of CzCzPh and **CzCzPh-mAd** in (a) film and (b) dichloromethane solution (1×10^{-5} M).

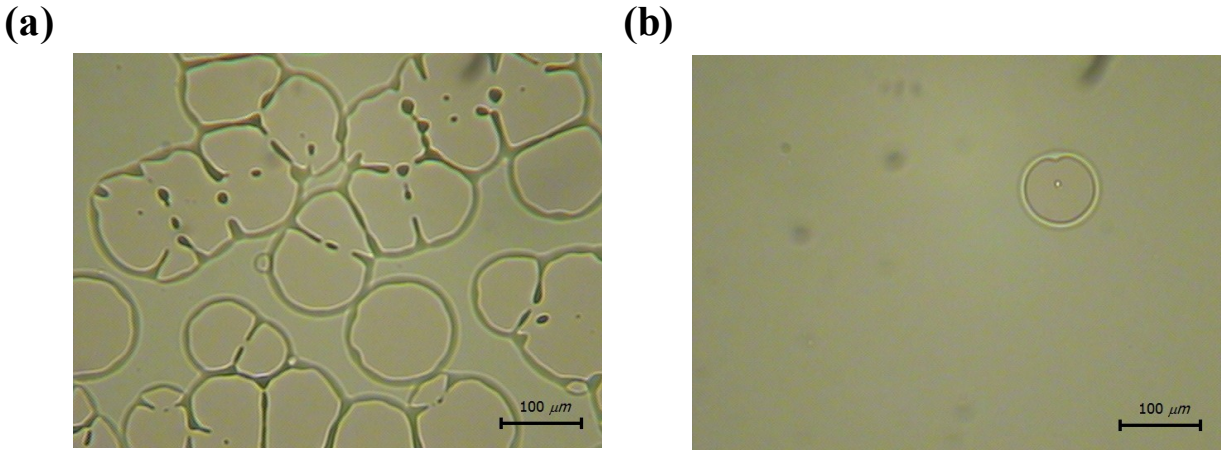

Fig. S9 Optical microscope images (a) CzCzPh and (b) **CzCzPh-mAd** films doped with 4 wt% 4FlCzBN after drying at 110 °C for 10 min.

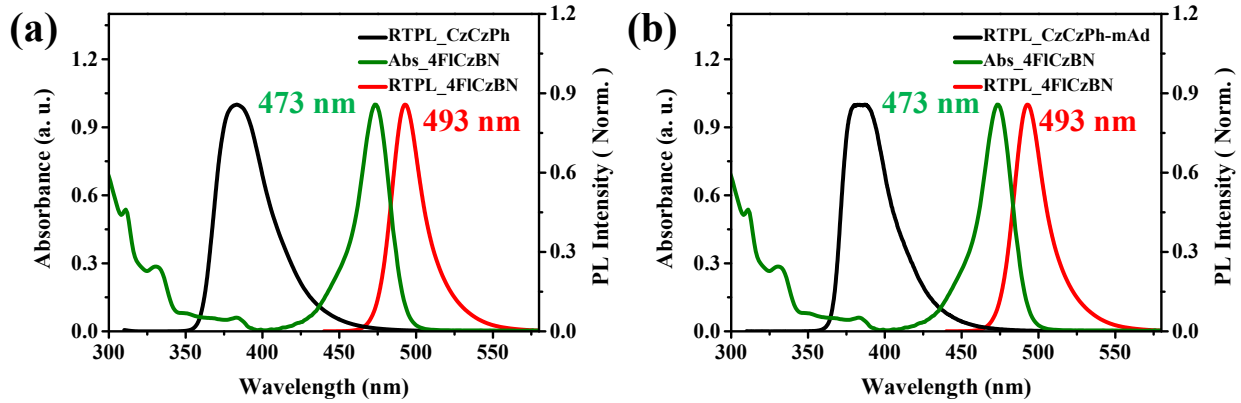

Fig. S10 UV-vis absorption (Abs, measured at 298 K) and fluorescence (RTPL, measured at 298 K) spectra of 4FICzBN and fluorescence (RTPL, measured at 298 K) of (a) CzCzPh and (b) **CzCzPh-mAd** in solution (toluene; 1.0 x 10^{-5} M).

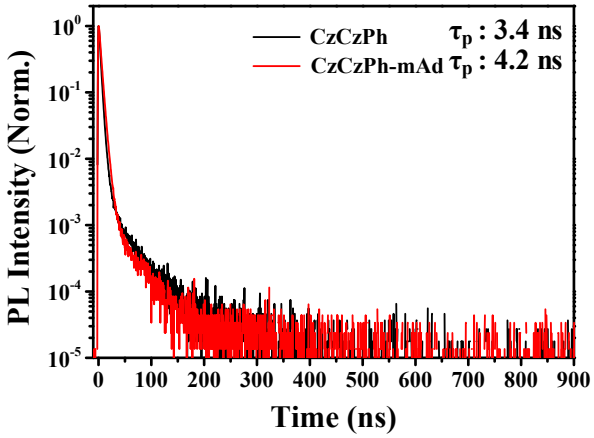

Fig. S11 TRPL signals measured at room temperature for thin films fabricated using CzCzPh and **CzCzPh-mAd**.

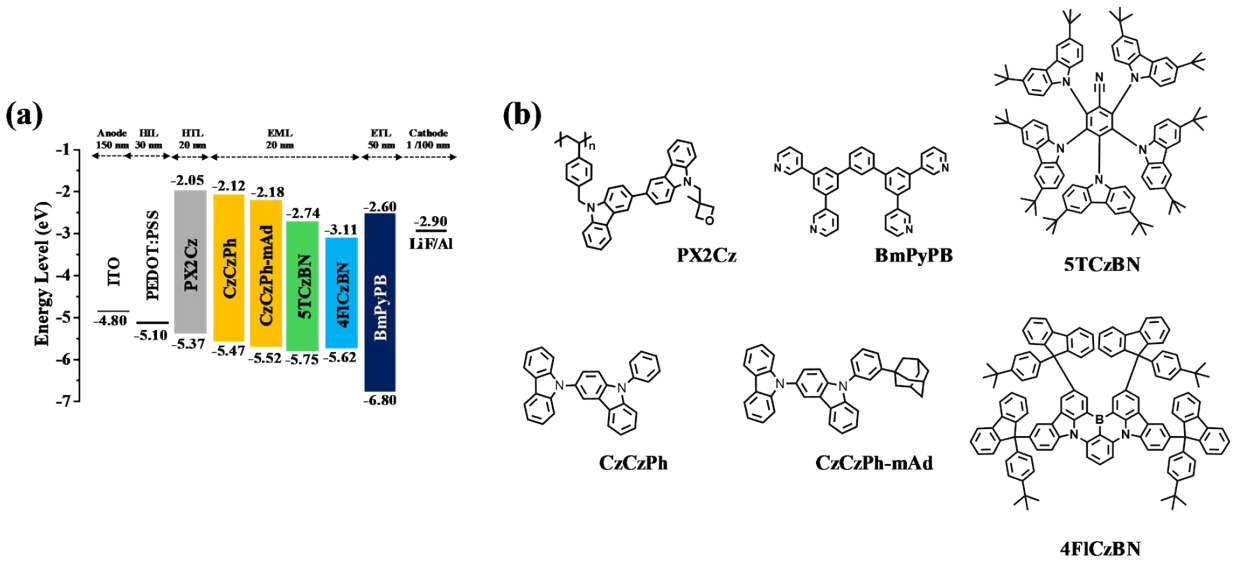

Fig. S12 (a) Device configurations and energy diagram of the solution-processed TADF-OLEDs. (b) Chemical structures of the materials employed in the devices.

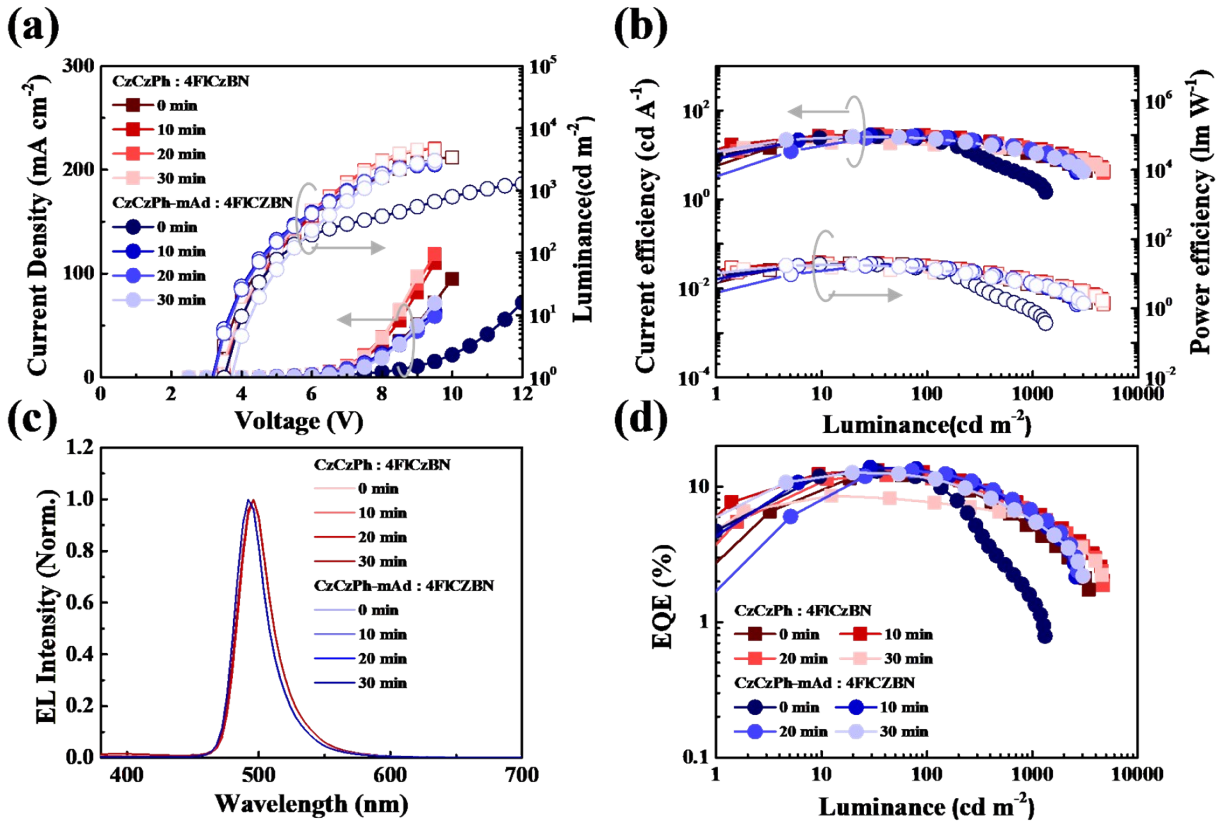

Fig. S13 (a) Current density–voltage–luminance (J–V–L) curves and (b) current efficiency–current density–power efficiency (CE–J–PE) curve. (c) EL spectra of CzCzPh and **CzCzPh-mAd** devices doped with 4 wt% 4FlCzBN after thermal drying at 120 ℃ for 0, 10, 20, and 30 min. (d) External quantum efficiency (EQE) curves of the devices.

Table S1 EL performance of the solution-processed TADF-OLEDs based on CzCzPh and **CzCzPh-mAd** at 4 wt% 4FlCzBN.

Host	Thermal Drying Condition	V_{on} [a] (V)	$\eta_{c,max}$ [b] (cd A^{-1})	$\eta_{p,max}$ [c] (lm W^{-1})	L [d] (cd m^{-2})	$\eta_{ext,max}$ [e] (%)	λ_{EL} [f] (nm)	FWHM (nm)	CIE [g] (x, y)
CzCzPh	120 ℃ 0 min	3.1	26.6	18.6	3434	12.1	496	29	(0.09,0.51)
	120 ℃ 10 min	3.3	29.3	20.4	4702	13.2	496	29	(0.09,0.51)
	120 ℃ 20 min	3.3	26.9	18.8	4681	12.1	496	29	(0.09,0.51)
	120 ℃ 30 min	3.3	19.0	15.0	4568	8.5	496	30	(0.09,0.51)
CzCzPh-mAd	120 ℃ 0 min	3.5	26.2	18.3	1324	13.0	492	27	(0.08,0.46)
	120 ℃ 10 min	3.5	27.8	19.4	2611	13.8	492	27	(0.08,0.46)
	120 ℃ 20 min	3.5	26.1	16.4	2706	13.1	492	27	(0.08,0.46)
	120 ℃ 30 min	3.5	25.9	18.1	3033	12.7	492	27	(0.08,0.46)

[a] Turn-on voltage of 1 cd m^{-2}. [b] Maximum CE. [c] Maximum PE. [d] Maximum luminance. [e] Maximum EQE. [f] EL peak wavelength.
[g] CIE color coordinates at 1000 cd m^{-2}.

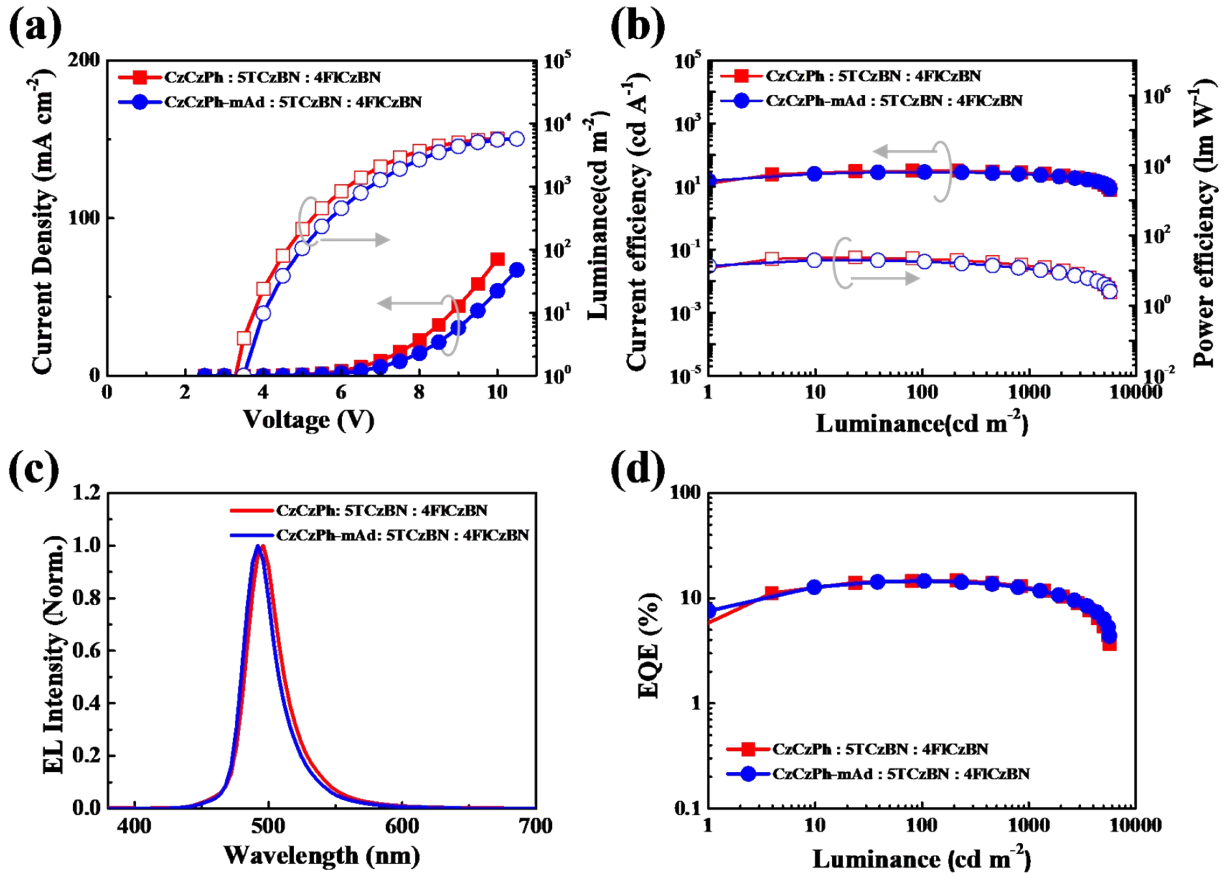

Fig.S14 (a) Current density–voltage–luminance (J–V–L) curves and (b) current efficiency–current density–power efficiency (CE–J–PE) curve. (c) EL spectra of the CzCzPh and **CzCzPh-mAd** films doped with 4 wt% 4FlCzBN and 20 wt% 5TCzBN. (d) External quantum efficiency curves of the devices of CzCzPh and **CzCzPh-mAd** doped with 4 wt% 4FlCzBN and 20 wt% 5TCzBN.

Table S2 EL performance of the solution-processed TADF-OLEDs based on 20 wt% 5TCzBN and 4 wt% 4FlCzBN : Hosts after thermal drying at 120 °C for 10min.

Host	Sensitizer	Emitter	V_{on} [a] (V)	$\eta_{c,max}$ [b] (cd A^{-1})	$\eta_{p,max}$ [c] (lm W^{-1})	L [d] (cd m^{-2})	$\eta_{ext,max}$ [e] (%)	λ_{EL} [f] (nm)	FWHM (nm)	CIE [g] (x, y)
CzCzPh	5tCzBN 20 wt%	4FlCzBN	3.11	31.5	19.8	5721	14.7	496	29	(0.10,0.48)
CzCzPh-mAd			3.49	28.7	18.0	5679	14.6	492	27	(0.09,0.43)

[a] Turn-on voltage of 1 cd m^{-2}. [b] Maximum CE. [c] Maximum PE. [d] Maximum luminance. [e] Maximum EQE. [f] EL peak wavelength. [g] CIE color coordinates at 1000 cd m^{-2}.

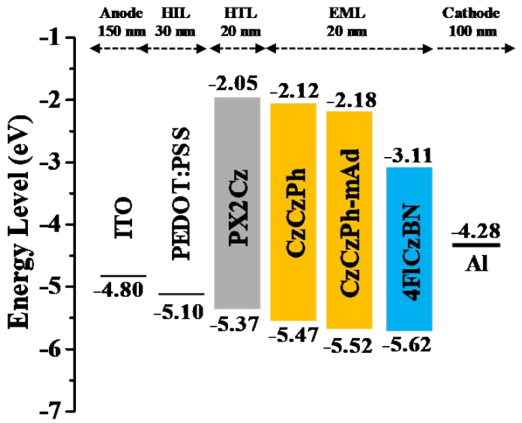

Fig. S15 Device configuration and energy diagram of the hole-only device (emitter: 4FlCzBN, concentration: 4 wt%).

■ REFERENCES

S1. R. Yu, F. Yin, C. Pu, D. Zhou, W. Ji, *Opt. Lett.*, 2023, **48**, 11.

S2. M. Xu, Q. Peng, W. Zou, L. Gu, L. Zu, L. Cheng, Y. He, M. Yang, N. Wang, W. Huang, J. Wang, *Appl. Phys. Lett.,*2019, **115**, 041102.

S3. J. H. Lee, C. H. Jeong, M. Godumala, C. Y. Kim, H. J. Kim, J. H. Hwang, Y. W. Kim, D. H. Choi, M. J. Cho, D. H. Choi, *J. Mater. Chem. C*, 2020, **8**, 4572

S4. N. Peethani, N. Y. Kwon, C. W. Koh, S. H. Park, J. M. Ha, M. J. Cho, H. Y. Woo, S. Park, D. H. Choi, *Adv. Opt. Mater.*, 2024, **42**, 2301217